RSC Advances

ROYAL SOCIETY OF CHEMISTRY

www.rsc.org/advances

Studies on the enhanced properties of nanocrystalline Zn-Ni coatings from a new alkaline bath due to the additives

Zhongbao Feng, Qingyang Li, Jinqiu Zhang, Peixia Yang, Maozhong An*

State Key Laboratory of Urban Water Resource and Environment, School of Chemical Engineering and Technology, Harbin Institute of Technology, Harbin 150001, China

Abstract: The effective composite additives coumarin (CA) and vanillin (VL) were used to electrodeposit nanocrystalline Zn-Ni alloys in a novel alkaline bath containing 5,5'-dimethylhydantoin (DMH) as the complexing agent. Similarly to the cyanide bath, an excellent mirror-like bright Zn-Ni alloy deposit with smooth, compact morphology and good leveling capability can be obtained from the newly developed bath with the composite additives. One cathodic peak of cyclic voltammogram (CV) curves indicates a single step two-electron transfer mechanism of Zn^{2+} and Ni^{2+}. The inhibition effect of VL is more pronounced than that of CA in the electrolyte through preferential adsorption on the cathode. larger cathodic polarization and finer grains are observed with the increase of VL than that of CA, indicating that VL is a main brightening agent. However, CA has a more prominent effect on the structure of Zn-Ni alloys compared to VL, which can be considered as a brightening promoter. The mechanisms of the decrease in grain size are considered in the bath with the addition of the composite additives. No oxidized zinc exists in the bulk of deposits by X-ray photoelectron spectroscopy (XPS) analysis. Moreover, mechanical, wear and corrosion resistance properties of Zn-Ni coatings were directly dependent on Ni content in deposits. The lower Ni content of bright coatings with smoother appearance

* Corresponding author. Tel: +86-451-86418616; Fax: +86-451-86418616.
E-mail addresses: mzan@hit.edu.cn (M.Z. An).

is obtained with composite additives and the bright coatings display more excellent wear and corrosion resistance than the dull coatings. The composite additives have the synergistic effect to significantly improve the properties of dull Zn-Ni alloys. Thus, the introduced new alkaline bath is a promising replacement for the conventional cyanide Zn-Ni alloy bath.

1. Introduction

Zn-Ni alloy coatings have attracted great interests in many applications due to their advantages such as anti-oxidation at high temperature,[1] higher hardness, better corrosion and wear resistance.[2] They are widely used as replacements for Zn and Cd[3,4] coatings in electrical, aerospace and industrial applications owing to their good corrosion resistance and environmental friendly properties. It is known that Zn-Ni alloy coatings with 8 to 14 wt.% of nickel and single gamma phase structure have higher corrosion resistance of five times compared to the pure Zn coatings.[5] The parameters in electrodepositing like the composition of the bath, current density, temperature and agitation speed significantly affect the microstructure and mechanical properties of Zn-Ni alloys.[6] This is due to that these parameters affect the Ni content in deposits, leading to the difference in the properties of Zn-Ni alloys.

Zn-Ni alloys have been successfully electrodeposited from the acid bath.[7,,8] But in general, most of the acid bath suffers from the poor throwing power. The bright Zn-Ni coatings with high corrosion resistance have been realized from alkaline cyanide bath. Unfortunately, cyanide is the toxic chemicals, which is great harmful to human and environment. To solve this problem, many attempts have been made to develop the alkaline non-cyanide bath. In recent years, a number of complexing agents have been proposed, such as amine,[9] ethylenediamine,[10] tartrate,[11] triethanolamine,[12] glycinate,[13,14] sodium acetate,[15,16] urea and citrate. However, these baths have a

relatively low current efficiency, leaving it impossible for commercial use. 5,5'-dimethylhydantoin (DMH) has been successfully used in Au,[17] Ag[18] and Cu[19] electrodeposition and it is a promising complexing agent in Zn-Ni alloy deposition owing to the large stability constants of DMH with Zn^{2+} and Ni^{2+}.[20] According to our previous studies,[6,21] the investigated new alkaline Zn-Ni alloy bath has a high stability and the aged baths have little effect on the electrochemical behaviors of the investigated electrolyte. Furthermore, the rate controlling step of the bath is a mixed controlled process and the actual nucleus growth of Zn-Ni alloys corresponds to the progressive nucleation process. However, to the best of our knowledge, DMH used as a complexing agent in Zn-Ni alloy deposition has not been reported up to now.

The properties of Zn-Ni alloys depend on the Ni content and grain size in deposits. The increase of Ni content in deposits can result in the increase in the microhardness of Zn-Ni alloys.[22] Nanocrystalline coatings exhibit superior characteristics that are not typically found in conventional coatings.[23] Excellent wear resistance[24], corrosion resistance[25] and better electrochemical properties[26] are obtained in nanocrystalline coatings compared with conventional polycrystalline deposits. Alfantez et al.[27] produced nanocrystalline Zn-Ni coatings from a chloride-based electrolyte and Li et al. [28] prepared nanocrystalline Zn-Ni coatings using a laboratory-made additive in alkaline bath. Their results showed finer grains and better corrosion resistance of nanocrystalline Zn-Ni alloys. Generally, nanocrystalline Zn-Ni alloys were obtained by adding additives into the basic bath during electrodepositing. Therefore, the addition of the additives is quite an efficiency way to reduce grain size and improve the properties of Zn-Ni alloys. Saccharin plays a very important role in the Ni based alloy deposition.[29] Mosavat et al.[14] studied the effect of saccharin on the crystallite size and surface roughness of deposits and found that the increase of saccharin led to

a decrease in crystallite size and surface roughness of deposits. The synergistic effect of gelatin and glycerol on the electrocrystalline process and corrosion stability of Zn-Ni alloys was studied by Rao et al.[30]. Muresan et al.[12] used coumarin, piperonal and vanillin as the additives. Their results showed that the fine grain Zn-Ni coatings exhibited best corrosion resistance with the addition of PEG and piperonal or vanillin. As a result, it is noted that the additives play a very important role in improving the properties of Zn-Ni alloys, but less focus is given to study them. Hence, it is essential to investigate the effect of the additives on Zn-Ni alloy deposition.

Up to now, a number of investigations have focused on the properties of Zn-Ni alloys by using different complexing agents. But no work was made by using DMH as the complexing agent and rare studies were studied the mechanical properties of deposits. In the present work, DMH is used as the complexing agent in the alkaine bath. Nanocrystalline Zn-Ni alloys were obtained in the presence of additives and the effect of additives on the potentiodynamic polarization curves, macroscopic images, surface morphologies, surface roughness, Ni content and current efficiency of deposits was investigated. Specially, the effect of the additives on the hardness, wear and corrosion resistance of deposits was studied.

2. Experimental

2.1. Electrodeposition and Electrochemical testing

Zn-Ni alloys were electrodeposited by direct current. The basic bath is consisted of $ZnSO_4 \cdot 7H_2O$ 70 g/L, $NiSO_4 \cdot 6H_2O$ 30 g/L, DMH 140 g/L, $Na_4P_2O_7 \cdot 10H_2O$ 40 g/L, and K_2CO_3 95 g/L. The composite additives coumarin and vanillin were introduced. In our research, coumarin and vanillin were recorded as CA and VL, respectively. The concentration of CA and VL was both in the range of 0-25 mg/L. The pH of the bath was adjusted to 9 ~ 10 by 10% sodium hydroxide solution, the current density was 2

A/dm^2 and the bath temperature was maintained at 50 ℃. The agitation speed was 1000 rpm. The electroplating time was 30 min. The cathodic substrates were carbon steel plates of 5 cm × 4 cm, which were degreased with 30 wt.% sodium hydroxide solution at 50 ℃ for 5 minutes, then activated with 50% hydrochloric acid for few seconds. After each step, the carbon steel plates were washed by distilled water. After electrodepositing, Zn-Ni alloy coatings were washed by distilled water, and dried by cold air.

The cathodic efficiency of electrodeposition (η) was calculated by Faraday's law according to the equation (1), using deposit composition, charge passed and weight gained of the deposit.

$$\eta = \frac{(m_2 - m_1)F}{I \cdot t} \sum \frac{c_i n_i}{M_i} \times 100\% \quad (1)$$

Where m_1 (g) and m_2 (g) are the weight before and after electroplating, I (A) is the total current passed in the plating time t (s), c_i is the weight fraction of the element in the Zn-Ni alloy deposit, n_i is the number of electrons transferred per atom of each metal, M_i is the molar mass of metal (g·mol^{-1}), and F is the Faraday's constant (96,485 C·mol^{-1}).

The Haring-Blum studies were employed to investigate the throwing power (T) of the bath. The throwing power was calculated by the following equation.

$$T = \frac{K - \frac{m_1}{m_2}}{K + \frac{m_1}{m_2} - 2} \times 100\% \quad (2)$$

Where T is the throwing power, K is the ratio between the respective distance of the far and near cathode from anode (5), m_1 and m_2 are the weight of Zn-Ni alloy deposits obtained from the near and far cathode, respectively.

Cyclic voltammetry (CV) and linear sweep voltammetry (LSV) were performed in a three-electrode cell using a CHI750D electrochemical workstation at 50 °C. A Pt electrode with a diameter of 3 mm was used as the working electrode (WE). The counter electrode (CE) was a platinum foil with an area of 1 cm^2. A mercury/mercurous sulfate electrode (SSE), i.e. Hg/Hg_2SO_4 was employed as the reference electrode (RE). The scan of CV and LSV was initiated at the open circuit potential (-0.3 V) with the scan rate of 150 mV/s and 1 mV/s, respectively.

2.2 Characterization of coatings

Scanning electron microscope (SEM, Helios Nanolab 600i) with energy dispersive X-ray spectroscopy (EDS) facility was employed to determine the surface morphology and Ni content in deposits, respectively. An atomic force microscope (AFM, Bruker) was used to study the surface roughness of Zn-Ni alloy coatings. The AFM analysis was carried out in the contact mode with silicon nitride cantilevers. The Hull cell of 267 mL capacity was used to study the brightness range and morphology of deposits. X-ray diffraction (XRD, D/max-γβ) was employed to analyze the phase structure, crystal orientation and average grain size of deposits with Cu Kα radiation at 40 kV and 40 mA. (λ = 0.1546 nm). The 2θ ranged from 20^o to 100^o at a scan rate of 0.02^o per second. The grain size was calculated by Scherrer's formula.

$$D=k\lambda/\beta\cos\theta \quad (3)$$

Where D is the average grain size of the coatings (nm), k is a constant (0.89), β is the full width at the half maximum (FWHM) and θ is the diffraction angle.

The hardness of deposits was measured by the nanoindentation tests (nanoindenter XP, MTS Systems Corporation). The penetration depth was 1 μm with a Berkovich diamond indenter. Five indents were made for each coating. After that, the average value was calculated. For the friction coefficients tests, a ball-on-disk tribometer

(Center for Tribology, HIT, China) was used. The Zn-Ni deposits discs were sliding against a stationary sphere of the counter material. The counter material used in this study was a 52100 steel ball with a diameter of 10 mm. The applied normal load was 1N and the sliding speed was kept constant at 7.9 cm/s for all tests. The tests were done in air at room temperature with a relative humidity of about 40%. With the help of a PC, the friction coefficient was continuously recorded during the tests. No lubrication was used during the wear tests.

The oxidation states of Zn and Ni in deposits were examined by X-ray photoelectron spectroscopy (XPS). A PHI 5700 ESCA System (Physical Electronics, USA) was employed to measure the XPS at the room temperature. The excitation source was Al Ka (alpha in Greek) radiation (photoelectron energy, 1486.6 eV) and the photoelectrons were detected with a hemispherical analyzer. The binding energies of the narrow scan and wide scan were determined at the pass energy of 29.35 eV and 187.85 eV with a resolution of ±0.3 eV, respectively. During sputtering, the accelerating voltage was 3kV, sputtering area was 4 mm × 4 mm, sputtering current was 0.5 μA and sputtering depth was 10 nm. The corrosion resistance of Zn-Ni alloy coatings was measured by the corrosion potentials and Tafel curves on a CHI750D electrochemical workstation at room temperature (25 °C) in 3.5 % NaCl solution, using a saturated calomel electrode (SCE) as the reference electrode, a platinum foil (1×1 cm^2) as the counter electrode, and 1 cm^2 area of carbon steel plates and Zn-Ni alloy coatings as the working electrodes. The scan rate of the curves was 1 mV/s with the scan range from -0.25 V to +0.25 V of open circuit potential. High purity nitrogen was used for deaeration of the solution. The luggin capillary was used to connect the reference electrode and working electrode. Also, the electrochemical workstation can compensate the IR drop automatically.

3. Results and discussion

3.1 Effects of CA and VL on CV and LSV curves

Cyclic voltammetry and linear sweep voltammetry have been used to investigate the influence of CA and VL in the Zn-Ni bath by adding nothing, 15 mg/L CA, 15 mg/L VL and both 15 mg/L CA and 15 mg/L VL, respectively. The standard potentials of Zn and Ni are -0.76 V and -0.25 V vs. SHE, respectively. As shown in Fig. 1a, the presence of the additive molecules has a significant effect on the shape of the voltammogram and also on the peak potential and current intensity values. It can be noted that the Zn-Ni alloy deposition on Pt electrode starts at approximately -1.25 V and the hydrogen evolution occurs along with Zn-Ni alloy deposition in the basic bath. The anodic sweep shows two dissolution peaks at A2 and A3. The multiple anodic peaks are attributed to the sequential oxidation of the different phases according to the literature.[31] Thus, the A2 is related to Zn dissolution from the γ phase (γ-Ni_5Zn_{21}), and A3 is due to the dissolution of the porous Ni matrix left after the preferential stripping of Zn from the γ phase. The Zn-Ni deposition shifts to more negative potential (starts at -1.3 V) and no significant change is observed in the shape of the CV curve with the addition of 15 mg/L CA (Fig. 1b'). But the associated current decreases, indicating that CA can adsorb on the cathode surface and inhibit the deposition of Zn-Ni alloy by blocking the available active sites. This inhibition is associated to the type and size of the organic molecules, and the specific interaction between the additives and the substrate.[11] The presence of VL in the bath changes the behavior of the voltammogram significantly. The deposition potential decreases to approximately -1.45 V and a cathodic peak C is recorded in Fig 1c'. This can be due to the strong inhibition of VL on Pt electrode surface. When the applied potential is large enough (> -1.78 V), the deposition rate of Zn^{2+} and Ni^{2+} occurred at the interaction

196 between the electrolyte and electrode surface is larger than the diffusion rate of Zn^{2+}
197 and Ni^{2+}. Thus, the concentration polarization appears and the diffusion current
198 decreases, resulting in the appearance of the cathodic peak C. After the peak C, the
199 increase in the current is due to the hydrogen evolution. The current crossover is
200 observed in the cathodic region, indicating the nucleation and growth of Zn-Ni
201 alloys.[32,33] In the anodic sweep, a new anodic peak A1 (-1.58 V) appears, which is
202 attributed to the stripping of Zn from η phase. When both CA and VL are present in
203 the bath (Fig. 1d'), the deposition potential is similar to that with only VL in the bath
204 (Fig. 1c'), indicating that the effect of VL is more pronounced than that of CA through
205 preferential adsorption on the cathode surface. The intensity of the peaks C, A1, A2
206 and A3 in Fig. 1d' decreases compared to the rest three curves. The improved
207 corrosion resistance of deposits is obtained owing to the decrease in the anodic
208 reactions.[34] Moreover, only cathodic peak C is associated with Zn-Ni alloy deposition
209 in Fig. 1d', indicating a single step two-electron transfer process of Zn^{2+} and Ni^{2+} in
210 Zn-Ni alloy deposition with the addition of both CA and VL.

211 As seen in Fig. 1b, the addition of CA and VL increases the cathodic polarization,
212 respectively. This can be explained by the inhibition effects of CA and VL at the
213 cathode, which is mentioned before. The presence of VL leads to greater cathodic
214 polarization compared with CA. The relative smaller difference between Fig. 1c" and
215 Fig.1d" is favor of the analysis that VL tend to adsorb preferentially on the cathode. In
216 general, CA and VL have a synergetic effect on the CV and LSV curves.

217 **Fig. 1**

218 **3.2 Effects of CA and VL on microstructure and surface morphologies of deposits**

219 To confirm the grain size and phase orientations of deposits, XRD patterns of
220 Zn-Ni alloys were investigated. It is well known that deposits often contain some

metastable phases and the phases that are deficient or oversaturated compared with their counterparts in the equilibrium phase diagram.[34] As shown in Fig. 2, the crystalline structure of deposits is observed. In the basic bath, XRD pattern shows an average grain size of 73.6 nm and two obvious diffraction peaks of γ phase (Ni_5Zn_{21}) with (411) and (721) plane orientations can be observed. With the addition of 15 mg/L CA, the grain size decreases to 62.1 nm. (721) plane disappears and (444) plane appears. Moreover, another γ phase ($NiZn_3$) with (1300) plane orientation appears. Because of the different potentials of these two phases (γ-Ni_5Zn_{21} and γ-$NiZn_3$), the electrochemical corrosion may occur in corrosive environments.[11] When only VL is added to the basic bath, (822) plane appears and the intensity of (411) plane increases. The average grain size of deposits is 48.5 nm. The more intense peak along (411) plane in Fig. 2d reveals that the coatings are textured along (411) plane. The deposits exhibit a crystallite size of 31.3 nm, which means that finer grain with single γ phase (γ-Ni_5Zn_{21}) of deposits can be obtained with the addition of the composite additives. This behavior proves the synergistic effects of CA and VL.

Fig. 2

In order to identify the effects of CA and VL on the crystalline grain size of Zn-Ni alloys, the mechanisms of the decrease in grain size are considered. To have finer grain size, the nucleation should be favored over growth. The overpotential is the most important factor during the decrease of the grain size, owing to faster nucleation rate at higher overpotential.[14] The nucleation rate v can be written as:

$$v=a \exp(-b/\eta) \quad (4)$$

Where a and b are overpotential-independent parameters, η is the overpotential. The nucleation law can be expressed as:

$$N=N_0 [1-\exp(-vt)] \quad (5)$$

Where N is the surface density of nuclei and N_0 is the respective saturation value. In order to increase the overpotential, the use of the additives is necessary. Mouanga et al.[35] have studied that CA can shift the potentials to more negative direction and obtain a large overpotential in Zn-Co deposition. We have also found that CA or VL can increase the overpotential in the investigated bath (shown in Fig. 1b). Thus, nucleation rate increases and results in the increase of the surface density of nuclei (Eq. (5)) according to Eq. (4). Therefore, the grain size decreases with the addition of CA or VL. A larger cathodic polarization of VL compared to CA (Fig. 1b) is observed, indicating the finer grain of deposits with VL. On the other hand, in the basic bath, the relative fine grain (< 100 nm) and large cathodic polarization are mainly related to the strong coordinated action between DMH and Zn^{2+} or Ni^{2+}. Therefore, DMH is a promising complexing agent in Zn-Ni alloy deposition.

The current of 2 A is used in the Hull cell studies, the brightness range of Zn-Ni alloy coatings obtained from the bath with the addition of composite additives at various contents of bath composition can be seen in Fig. S1 (in the supporting information). It is observed that the brightness range of deposits increases with the increase of DMH content, $Na_4P_2O_7 \cdot 10H_2O$ content and K_2CO_3 content in the bath, respectively. However, the bright deposits in the range of 1-10 A/dm^2 only can be seen in the appropriate $Ni^{2+}/(Zn^{2+}+Ni^{2+})$ ratio (0.32) or $(Zn^{2+}+Ni^{2+})$ content (100 g/L) (Fig. S1c-d). Furthermore, the surface morphologies of Zn-Ni alloy coatings deposited from the bath with additives at various concentrations of the bath composition are shown in Fig. S2-S6. It is noted that the coarse grains of Zn-Ni alloy coatings are observed at low DMH content (120 g/L), and the fine and uniform grains can be seen with the increase of DMH content from 140-160 g/L (Fig. S2). In contrast, The $Na_4P_2O_7 \cdot 10H_2O$ content has little effect on the surface morphologies of Zn-Ni alloy

deposits. The fine and uniform grains are observed in the range of 30-50 g/L $Na_4P_2O_7 \cdot 10H_2O$ content in the bath (Fig. S3). Thus, it is concluded that DMH has a grain refining effect and acts as the main complexing agent in the bath. This is in accordance with the XRD results (Fig. 2). The grain size of deposits increases with the increase of $Ni^{2+}/(Zn^{2+}+Ni^{2+})$ ratio and $(Zn^{2+}+Ni^{2+})$ content, respectively (Fig S4-S5). However, the grain size of deposits is nearly constant when the K_2CO_3 content increases from 75 g/L to 115 g/L (Fig. S6).

Bright Zn-Ni alloy coatings can be obtained at 1-10 $A \cdot dm^{-2}$ from the baths with the addition of 5-25 mg/L CA and 5-25 mg/L VL to the basic bath. Fig. 3 reveals the surface morphologies of Zn-Ni alloys with different baths by adding nothing or the additives, respectively. As shown in Fig. 3a, the coatings show rod-like clusters with an uneven size in the basic bath. With the addition of 15 mg/L CA, the deposits are composed by some agglomerations (Fig.3b) and some finer grains (triangular pyramid) can be observed at the boundary of the coarser agglomerations. Furthermore, the deposits with 15 mg/L VL (Fig. 3c) display the dendritic-like morphologies and the grain of deposits is uniform and smaller than that of the coatings shown in Fig. 3a and b. These behaviors indicate that CA or VL can promote the formation of fresh nucleation sites and hinder the growth of nuclei during deposition, leading to the refinement of grain size in deposits. However, VL plays a more important role in the surface morphology and grain size of deposits owing to the preferential adsorption on the cathode. The results are in accordance with the analysis of the LSV and XRD curves shown in Fig. 1 and 2. By comparison, when both CA and VL are added in the bath, a significant decrease of the grain size can be observed and the deposits are smooth, uniform compact and fine grained without any pores or pinholes at the surface (Fig. 3d), suggesting the synergetic effects of CA and VL. On the other hand,

the grain size decreases and the deposits become smoother with the increase of the concentration of the CA and VL, respectively, (Fig. S7 and Fig. S8).

Fig. 3

The surface properties of Zn-Ni alloys were also studied with AFM measurement. As seen in Fig. 4, Zn-Ni alloys obtained from the basic bath without additives show a rough and heterogeneous surface with large crystal grains. While Zn-Ni alloys obtained from the bath with additives (15 mg/L CA and 15 mg/L VL) exhibit smoother and more homogeneous surface with smaller crystal grains. Furthermore, the surface roughness of the bright coatings (Fig. 4b, Rq=17.1 nm, Ra=13.7 nm, Rmax=112 nm) is much lower than that of the dull coatings (Fig. 4a, Rq=54.4 nm, Ra=43.1 nm, Rmax=319 nm). According to the section analysis of the surface of deposits (Fig. S9c), it can also be seen that the bright coatings also have the more homogeneous surface compared to the dull coatings, indicating that the investigated Zn-Ni alloy bath exhibits excellent leveling capability with the addition of composite additives. This can be explained by the fact that the protuberance of the cathode surface has higher current densities and the additives are adsorbed on these regions preferentially and inhibit Zn-Ni alloy deposition, resulting in the smaller reduction of Zn^{2+} and Ni^{2+} on these points. Therefore, the smoother and brighter deposits can be observed.[11] As a result, the surface of deposits goes from rough to smooth with the addition of composite additives due to the inhibition effects of additives during electroplating. Moreover, the surface roughness of Zn-Ni alloy coatings obtained from the bath with 15 mg/L CA and 15 mg/L VL is smaller than that of Zn-Ni alloy coatings obtained from the baths with other concentrations of CA and VL.

Fig. 4

The effects of additives on the appearance of Zn-Ni alloy deposits were

investigated. Fig. 5 shows the macroscopic images of Zn-Ni alloys obtained from the bath without and with the composite additives, respectively. When the Zn-Ni deposits are dull, it is difficult to be used as a replacement for Cd coatings, because the bright appearance is necessary in the most applications of Cd coatings. Additionally, the bright Zn-Ni alloys can also be used as the middle layer in decorative purposes and are benefit for the requirements of the passivation. Therefore, it is necessary to obtain the Zn-Ni alloy deposits with bright appearance. Fig. 5a and c are obtained from the basic bath without additives, which shows matt and pale-gray appearance with relatively rough surface. In contrast, with the addition of the composite additives (15 mg/L CA and 15 mg/L VL), a mirror-like bright appearance of Zn-Ni alloy with smooth surface is obtained as shown in Fig 5b and d, indicating that the introduced composite additives can significantly improve the appearance of Zn-Ni alloy surface. In addition, when only CA is added in the basic bath, the edge of the cathode is brighter than the center of it. However, the center of the cathode has a more mirror-like appearance with the addition of VL to the basic bath alone. Therefore, the combined of these two additives is necessary.

Fig. 5

It can be concluded from the above results that the addition of both CA and VL is better than that of them alone. CA and VL have a mutual promoted effect in Zn-Ni alloy deposition. The influence of VL is more pronounced than that of CA on the grain size of deposits and cathodic polarization through preferential adsorption at the cathode. The throwing power of the bath with the addition of the composite additives is 41.7%.

3.3 Effect of the concentration of CA and VL on compositions of Zn-Ni alloys.

Effect of different concentrations of CA and VL on LSV curves are shown in Fig.6a

and b, respectively. The cathodic polarization increases and the intensity of current peak decreases with the increase of the concentration of CA or VL from 5 mg/L to 15 mg/L. Fig. 6a shows the relatively larger value of current compared to that displayed in Fig. 6b, when the potential is in the same. This phenomenon is evidenced by the stronger inhibition effect of VL than that of CA. In addition, there is little difference between the curves obtained from the baths with 15 mg/L and 25 mg/L CA or VL, indicating that it is meaningless to increase the cathodic polarization by further increasing the concentration of CA or VL (> 15 mg/L). However, larger cathodic polarization can be observed in the bath with the composite additives (in contrast to Fig. 1d"). The results prove the fact that the use of the composite additives is a more effective way to obtain the bright Zn-Ni alloys than VL and CA can do individually.

Fig. 6

Fig. 7 reveals the effect of the concentration of CA and VL on Ni content and current efficiency from the bath with 15 mg/L VL and 15 mg/L CA, respectively. Ni content has little change at first and significantly decreases to 12.95 wt.% with the increase of CA from 0 to 25 mg/L. While Ni content of deposits first decreases then attains an average constant value of about 13.4 wt.% by increasing VL from 0 to 25 mg/L. These behaviors are due to the inhibition effects of CA and VL on the cathode. The reduction of Zn^{2+} and Ni^{2+} is inhibited by the barrier formed by CA or VL and the barrier is more difficult to pass through for Ni^{2+} than Zn^{2+}, resulting in the decrease of Ni content in deposits. The different tendency of Ni content caused by CA and VL can be evidenced by Fig. S10. When CA is in the range of 0 ~ 10 mg/L, there is little effect on the cathodic and anodic current. However, the current of cathodic and anodic scan decreases rapidly with the increase of CA from 10 ~ 20 mg/L. The behavior of CV curves is in accordance with the tendency of Ni content in deposits. In

correspondence, Ni content in deposits can also make a difference to the structure of deposits, resulting in the different voltammetric responces of CV curves.[31] Similarly, VL also has the same behavior. On the other hand, the current efficiency is over 85%, when the concentration of CA and VL is 15 mg/L and 15 mg/L, respectively. The current efficiency sharply decreases by about 10% with the increase of CA and VL from 0 mg/L to 25 mg/L, respectively. It is well known that the content of each metal in deposits is related to the partial current density induced by each discharge reaction in the case of alloy deposition.[36] The more sites of the cathode will be covered with the additives by increasing the concentration of CA or VL. Thus, the cathode polarization increases, leading to the decrease of the partial current density of Zn^{2+} and Ni^{2+}. As a result, the current efficiency decreases. In addition, the increase in viscosity of the bath is also a reason for the decrease of the current efficiency. The mass transport of Zn^{2+} and Ni^{2+} from bulk solution to the interface of the cathode and the solution is reduced, which decreases the deposition current density of Zn^{2+} and Ni^{2+}, consequently, decreases the current efficiency. A slight increase of current efficiency with 5 mg/L VL may be associated with the competition of VL and hydrogen for the active sites at the cathode, inhibiting the hydrogen evolution reaction. Pedroza et al[37] obtained the similar result with the addition of glycerol.

Fig. 7

In order to analysis the relationship between the concentration of CA or VL and the structure of deposits. X-ray diffraction patterns of deposits were studied. As seen in Fig. 8a. The deposits are consisted of γ phase. In addition to the γ phase with (1300) plane orientation is γ-$NiZn_3$, the rest γ phases are γ-Ni_5Zn_{21}. When CA increases from 5 mg/L to 15 mg/L, the intensity of γ phase with (411) plane orientation is larger than that of other peaks, indicating that the coatings have well preferred orientation along

(411) plane. However, the reflection corresponding to (411) plane is highly suppressed and the preferred orientation alters to (1300) plane with the increase of concentration of CA to 25 mg/L. Furthermore, γ phase with (444) plane orientation becomes obvious, indicating the large influence of the concentration of CA on the structure of Zn-Ni alloys. As seen in Fig. 8b, the concentration of VL has little effect on the structure of Zn-Ni alloys, the γ phase with (411) plane orientation plays a dominant role in deposits with the increase of concentration of VL from 5 to 25 mg/L. Also, the deposits with single phase can exhibit better corrosion resistance.[5] Therefore, it is concluded that CA has a more prominent effect on the structure of Zn-Ni alloys compared to VL.

The average grain size of deposits decreases from 43.9 nm to 27.6 nm in Fig. 8a and from 51.3 nm to 24.4 nm in Fig. 8b, indicating the grain refine effect with the increase of the concentration of CA or VL. The results show in good agreement with the analysis displayed in Fig. S7 and Fig. S8.

Fig. 8

3.4 Effect of the composite additives on mechanical performance of Zn-Ni alloys

Fig. 9 shows the effect of additives on the hardness distribution of Zn-Ni alloys. It is noted that the hardness of Zn-Ni alloys with and without additives is 3.55 GPa and 4.59 GPa, respectively, while the penetration depth is 1000 nm. Based on our previous studies,[6] the hardness of deposits is mainly dependent on Ni content and increases with the increase of Ni content in deposits. As shown in Fig. 7, Ni content decreases with the increase of additives. Thus, the hardness of deposits decreases when the composite additives are added in the basic bath. Even so, the hardness of deposits obtained with additives (about 424 HV_{100}) is significantly higher compared to other nanosrystalline Zn-Ni alloys (about 410 HV_{25}) obtained in general alkaline bath.[14]

421 **Fig. 9**

422 Tribological properties of Zn-Ni alloys were studied by friction coefficient. The
423 plots of friction coefficient values with the sliding distance on the surface of Zn-Ni
424 alloys obtained from the bath with and without additives are shown in Fig. 10. It is
425 clear that the friction coefficient first increases and then attains the value in the range
426 of 0.55 ~ 0.65. The values of the friction coefficient are relatively unstable, when no
427 additives are added in the bath. With the addition of the additives (15 mg/L CA and 15
428 mg/L VL), the friction coefficient remains a low value of 0.06 at the first stage of
429 wear, which is related to the mirror-like bright and smooth surface of the coatings. It
430 has been proved that the bright surface appearance and smooth morphology of
431 deposits can lead to the decrease in friction behavior.[22] Therefore, the low value of
432 friction coefficient is observed at the beginning of the wear test. When the friction
433 track appears, the debris and scratches appear and the surface of deposits becomes
434 relatively rough. This is accompanied by increasing the friction coefficient to 0.51.
435 Compared to the curves obtained from the bath without additives, the steady state
436 value of friction coefficient for coatings obtained with additives is lower and more
437 stable. This behavior is mainly due to the decrease of Ni content in deposits.
438 According to the results before, the smoother surface morphology and finer grain size
439 of deposits with lower Ni content are observed with the composite additives. The
440 analysis indicates that the bright coatings with low Ni content can decrease the
441 friction coefficient of deposits. Similar results were also reported for Ni-Co alloy with
442 decreased Ni content and reduced friction coefficient value by Lokhande et al.[29]
443 Generally speaking, under a certain load, the lower friction coefficient and smoother
444 appearance can result in the better wear resistance.[22] Thus, it can be concluded that
445 the coatings obtained from the bath with composite additives exhibit excellent friction

446 reduction effect than the coatings obtained from the bath without additives at the same
447 wear conditions.

448 **Fig. 10**

449 **3.5 The oxidation states of Zn and Ni in deposits**

450 To remove any oxidation products and surface impurities (mainly carbon), the
451 surface of Zn-Ni alloys was sputtered with Ar^+ ions. Fig. 11 shows the spectra of the
452 original surface and a 10.0 nm depth of Zn-Ni alloys, respectively. The survey scan is
453 taken over in a wide binding energy region from 1.2-1350 eV. It shows the presence
454 of zinc, nickel, carbon and oxygen. After a 10.0 nm depth of Ar^+ sputtering, zinc and
455 nickel dominate in the coatings. Moreover, nitrogen can also be found in deposits as
456 seen in Fig. 11b. The binding energy of the C1s peak at 284.6 eV is employed as an
457 internal standard.

458 The difference in binding energy between Zn^{2+} and metallic zinc is very small (0.1
459 eV). Thus, it is difficult to distinguish whether the zinc occurs at the (0) or (2+)
460 oxidation state. Therefore, the O1s spectrum can be used to determine the metallic
461 zinc and oxidized zinc. As displayed in Fig. 11e, two distinct peaks are found at the
462 binding energy of 531.5 and 529.9 eV in the original surface. The high binding energy
463 peak can be related to hydrogen-bonded oxygen, while the lower binding energy peak
464 indicates the presence of the metal-bonded oxygen.[38] The hydrogen-bonded oxygen
465 is mainly due to the adsorption of additives on Zn-Ni alloy surface. Fig. 11d shows
466 that Ni exists in the form of metallic nickel at 852.8 eV and 870.0 eV on the surface
467 and a 10.0 nm depth of Zn-Ni alloys,[39,40] respectively. Thus, the metal-bonded
468 oxygen proves the presence of oxidized zinc on the surface of Zn-Ni alloys. After a
469 10.0 nm depth of sputtering (Fig. 11f), only the binding energy of 531.5 eV appears in
470 O1s spectrum, indicating that the presence of oxygen is related to the inclusion of

additives in the bulk of deposits. Therefore, only metallic zinc and nickel remains in the bulk Zn-Ni alloys after Ar^+ sputtering. The difference of the binding energy of Zn2p in the original surface and a 10.0 nm depth of Zn-Ni alloys also confirms the above analysis. Some researchers[41] have found the oxidized zinc species in the bulk of Zn-Ni alloy deposits. This can be explained by the low current efficiency (about 40%) of the electrodeposition. The low current efficiency results in the large alkalization of the solution and causes the formation of oxidized zinc. When the current efficiency is over 80%, only metallic zinc occurs in deposits. In our investigation, the current efficiency is over 85% in the deposition and the zinc complexes are stable in the alkaline bath. It has been mentioned that DMH has large stability constants with Zn^{2+} and Ni^{2+}.[20] Moreover, the strong coordinated action between DMH and Zn^{2+} or Ni^{2+} is observed during electrodepositing, which is evidenced by the relative fine grain size in the basic bath (Fig. 2a). Therefore, only metallic zinc can be found in the bulk of Zn-Ni alloys. In addition, the presence of nitrogen on the surface is due to the fact that DMH is easy to adsorb at the cathode.[18] After sputtering, the presence of nitrogen is obvious, indicating that a small quantity of DMH can be found in the bulk of Zn-Ni alloys. Ni content on the surface and a 10.0 nm depth of Zn-Ni alloys is 12.97 wt.% and 13.41 wt.%, respectively, indicating the well-distribution of nickel content in the direction of cross section.

Fig. 11

3.6 Effect of composite additives on the corrosion resistance of Zn-Ni alloys

Zn-Ni alloys are the anodic coatings (the corrosion potential of the coatings is more negative compared to the substrate (steel)). The porosity of Zn-Ni coatings has little effect on the corrosion behaviors of the substrate. This can be explained by the fact that when the two metals (Zn-Ni alloy coatings and steel) form a bimetallic corrosion

cell through the porosity, Zn-Ni alloys will be corroded preferentially compared to the steel owing to the more negative corrosion potential of Zn-Ni alloys than that of the steel. Furthermore, the thickness of Zn-Ni alloy coatings is 15.82 μm after electrodepositing for 30 min. The porosity of the coatings decreases rapidly with the increase of the thickness of deposits,[42] resulting in the less contact between the Zn-Ni alloy coatings and the substrate. Thus, the corrosion decreases. The potential of 3 μm Zn-Ni alloy coatings remains nearly constant for 24 h in 3.5% NaCl solution at 25 °C. In contrast, the potentials of 6 μm and 15 μm thickness coatings remain constant for 96 h (Fig. S11). The analysis approves the above result that the porosity of the Zn-Ni coatings has little effect on the corrosion behaviors of the substrate.

Tafel plot is an important technique to determine the corrosion resistance of deposits. Fig. 12 shows the Tafel plots of Zn-Ni alloys obtained in the absence and presence of additives in a 3.5% NaCl solution. The electrochemical parameters (E_{corr}, i_{corr}, β_c, β_α) of deposits are summarized in Table 1. The corrosion potentials of these two Zn-Ni alloy deposits from corrosion experiments are more negative than that of steel product. This means that Zn-Ni alloy coatings can sacrificially protect the steel. Also, the bright coatings show more positive potential E_{corr} and lower i_{corr} values than the dull coatings, indicating the improvement in the corrosion resistance of the bright coatings. It is known that the corrosion resistance of Zn-Ni alloys is mainly related to the Ni content in deposits and the highest corrosion resistance is achieved when Ni content in deposits is about 13%.[43] When the composite additives are added in the basic bath, the adsorbed additives suppress the reduction of Ni^{2+} and the Ni content decreases from 15.16% to 13.42%. Thus, the enhanced corrosion protection of Zn-Ni alloys is achieved due to the additives. In addition, the higher binding energy of atoms is observed in the bright coatings compared to the dull coatings due to the large

available numbers of nearest neighboring atoms in the bright coatings. When the metal atoms are at the grain boundaries, they are more easily to be corroded due to the higher activity of the atoms. The volume fraction of the grain boundaries increases with the decrease of the grain size. Thus, the bright coatings exhibit better corrosion resistance compared to the dull coatings. Furthermore, the corrosion product layers on Zn-Ni alloys mainly consisted of $ZnCl_2 \cdot 4Zn(OH)_2$ and ZnO[44,45] are formed in NaCl medium during corrosion. The bright coatings are characterized by the finer grains, resulting in an increase of the number of the active atoms on the surface and this behavior will accelerate the formation of protective corrosion product layer. As a result, the enhanced stability of the dense and complete corrosion product forms on the surface of bright coatings during the corrosion. Therefore, better corrosion resistance of the bright coatings can be obtained from the bath with additives compared to the dull coatings obtained from the bath without additives.

Fig. 12

Table. 1

4. Conclusions

A novel alkaline bath is proposed to replace the cyanide bath in Zn-Ni alloy coatings. Coumarin (CA) and vanillin (VL) were employed as the composite additives. The results indicate that in addition to complexing, DMH has a second role in the electrolyte, which is grain refining. Only one cathodic peak is associated with Zn-Ni alloy deposition, indicating a single step two-electron transfer process of Zn^{2+} and Ni^{2+}. The presence of CA and VL has a strong effect on the properties of Zn-Ni alloys. The reduction of Zn^{2+} and Ni^{2+} is inhibited by the adsorption of CA and VL on the cathode surface and the inhibition action of VL is more pronounced than that of CA through preferential adsorption. Thus, VL is a main brightening agent in the bath. A

mirror-like bright Zn-Ni alloy deposit with smooth, compact morphology and excellent leveling capability can be obtained from the bath with the composite additives. The grain size, Ni content and current efficiency decrease with the increase of the concentration of CA or VL. This is due to the increase in the overpotential by the inhibition of additives. Compared to VL, CA has a more prominent effect on the structure of Zn-Ni alloys and can be considered as a brightening promoter.

The hardness of the bright coatings is lower than that of the dull coatings. This is related to Ni content in deposits. Even so, the hardness of the bright deposits (about 424 HV_{100}) is significant higher than that of other nanocrystalline Zn-Ni alloys (about 410 HV_{25}) obtained in general alkaline bath. The friction coefficient of the bright coatings with lower Ni content and smoother surface is lower and more stable compared to the dull deposits, indicating more excellent friction-reduction behavior and better anti-wear performance. Oxidized zinc and the adsorbed additives exist on the surface of Zn-Ni alloy deposits. While no oxidized zinc occurs in the bulk of deposits. The bright coatings exhibit much higher corrosion resistance than the dull coatings. This is mainly due to the proper Ni content (about 13 wt.%) and higher binding energy of atoms in bright deposits. Furthermore, the enhanced stability of corrosion product layers of the bright coatings can also increase the corrosion resistance.

CA and VL have a synergistic effect on the properties of deposits. The addition of the composite additives is a quite effective way to significantly improve the properties of Zn-Ni alloy deposits. Therefore, the investigated alkaline bath is innovative, simple, environmental friendly and can be used as a promising alternative to cyanide Zn-Ni alloy bath.

Acknowledgments

571 The authors are grateful for financial support from the State Key Laboratory of Urban
572 Water Resource and Environment (Harbin Institute of Technology) (2012DX03).

573 Notes and References

1 R.M. Gnanamuthu, S. Mohan, G. Saravanan and C.W. Lee, *J. Alloys Compd.*, 2012, **513**, 449.

2 K.R. Sriraman, H.W. Strauss, S. Brahimi, R.R. Chromik, J.A. Szpunar, J.H. Osborne and S. Yue, *Tribol. Int.*, 2012, **56**, 107.

3 D.A. Wright, N. Gage and B.A. Wilson, *Plating. Surf. Finish.*, 1994, **81**, 18.

4 G.F. Hsu, *Plating. Surf. Finish.*, 1984, **71**, 52.

5 Y. Boonyongmaneerat, S. Saenapitak and K. Saengkiettiyut, *J. Alloys Compd.*, 2009, **487**, 479.

6 Z.B. Feng, Q.Y. Li, J.Q. Zhang, P.X. Yang, H.L. Song and M.Z. An, *Surf. Coat. Technol.*, 2015, **270**, 47.

7 S.O. Pagotto, C.M. de Alvarenga Freire and M. Ballester, *Surf. Coat. Technol.*, 1999, **122**, 10.

8 S.S. Abd El Rehim, E.E. Fouad, S.M. Abd El Wahab and H.H.Hassan, *Electrochim. Acta*, 1996, **41**, 1413.

9 C. Müller, M. Sarret and M. Benballa, *J. Electroanal. Chem.*, 2002, **519**, 85.

10 H. Nakano, S. Arakawa, S. Oue and S Kobayashi, *ISIJ Int.*, 2013, **53**, 1864.

11 M.G. Hosseini, H. Ashassi-Sorkhabi and H.A.Y. Ghiasvand, *Surf. Coat. Technol.*, 2008, **202**, 2897.

12 L.M. Muresan, J. Eymard, D. Blejan and E. Indrea, *Stud. Univ. Babes-Bolyai, Chem.*, 2010, **1**, 37.

13 L.S. Tsybulskaya, T.V. Gaevskaya, O.G. Purovskaya and T.V. Byk, *Surf. Coat.*

Technol., 2008, **203**, 234.

14 S.H. Mosavat, M.E. Bahrololoom and M.H. Shariat, *Appl. Surf. Sci.*, 2011, **257**, 8311.

15 H. Conrad, J. Corbett and T.D. Goldenz, *J. Electrochem. Soc.*, 2012, **159**, C29.

16 E. Beltowska-Lehman, P. Ozga, Z. Swiatek and C. Lupi, *Surf. Coat. Technol.*, 2002, **151-152**, 444.

17 X.W. Yang, M.Z. An., Y.W. Zhang and L. Zhang, *Electrochim. Acta*, 2011, **58**, 516.

18 A.M. Liu, X.F. Ren, B. Wang, J. Zhang, P.X. Yang, J.Q. Zhang and M.Z. An, *Rsc Adv.*, 2014, **4**, 40930.

19 J. Zhang, A.M. Liu, X.F. Ren, J.Q. Zhang, P.X. Yang and M.Z. An. *Rsc Adv.*, 2014, **4**, 38012.

20 G.Z. Pavlovich and R.G. Luthy, *Water Res.*, 1988, **22**, 327.

21 Z.B. Feng, Q.Y. Li, J.Q. Zhang, P.X. Yang, H.L. Song and M.Z. An, *J. Electrochem. Soc.*, 2015, **162,** D412.

22 S. Ghaziof and W. Gao, *Appl. Surf. Sci.*, 2014, **311**, 635.

23 I. Gurrappa and L. Binder, *Sci. Technol. Adv. Mater.*, 2008, **9**, 11.

24 U. Erb, *Nanostruc. Mater.*, 1995, **6**, 533.

25 R. Rofagha, R. Langer, A.M. El-Sherik, U. Erb, G. Palumbo and K.T. Aust, *Mater. Res. Soc. Symp. Proc*., 1992, **238**, 751.

26 L. Lu, Y. Shen, X. Chen, L. Qian and K. Lu, *Science*, 2004, **304**, 422.

27 A.M. Alfantazi and U. Erb, *J. Mater. Sci. Lett*., 1996, **15**, 1361.

28 G.Y. Li, J.S. Lian, L.Y. Niu and Z.H. Jiang, *Surf. Coat. Technol.*, 2005, **191**, 59.

29 A.C. Lokhande and J.S.Bagi, *Surf. Coat. Technol.*, 2014, **258**, 225.

30 V.R. Rao and A.C. Hegde, *Metall. Mater. Trans. B*, 2013, **44B**, 1236.

31 G. Trejo, R. Ortega, Y. Meas, E. Chainet and P. Ozil, *J. Appl. Electrochem.*, 2003 **33**, 373.

32 J.Q. Zhang, M.Z. An and L.M. Chang, *Electrochim. Acta*, 2009, **54**, 2883.

33 H.Y. Yang, X.W. Guo, X.B. Chen, S.H. Wang, G.H. Wu, W.J. Ding and N. Birbilis, *Electrochim. Acta*, 2012, **63**, 131.

34 A.C. Hegde, K. Venkatakrishna and N. Eliaz. *Surf. Coat. Technol.*, 2010, **205**, 2031.

35 M. Mouanga, L. Ricq and P. Berçot, *Surf. Coat. Technol.*, 2008, **202**, 1645.

36 J.Q. Zhang, M.Z. An, L.M. Chang and G.Y. Liu, *Electrochim. Acta*, 2008, **53**, 2637.

37 G.A.G. Pedroza, C.A.C. de Souza, I.A. Carlos and L.R.P. de Andrade Lima, *Surf. Coat. Technol.*, 2012, **206**, 2927.

38 B. Bozzini, E. Griskonis, A. Fanigliulo and A. Sulcius, *Surf. Coat. Technol.*, 2002, **154**, 294.

39 C.E. Dube, B. Workie, S.P. Kounaves, A. R. Jr., M.L. Aksub and G. Davies, *J. Electrochem. Soc.*, 1995, **142**, 3357.

40 L.S. Hsu and R.S. Williams, *J. Phys. Chem. Solids*, 1994, **55**, 305.

41 B. Szczygieł, A. Laszczyńska and W. Tylus, *Surf. Coat. Technol.*, 2010, **204**, 1438.

42 C. Kerr, S. Court, B.D. Barker, F.C. Walsh, *Surf. Coat. Technol.*, 2008, **202**, 5092.

43 S.H. Mosavat, M.H. Shariat and M.E. Bahrololoom, *Corros. Sci.*, 2012, **59**, 81.

44 Q. Qu, L. Li, W. Bai, C. Yan and C.N. Cao, *Corros. Sci.*, 2005, **47**, 2832.

45 N. Boshkov, *Surf. Coat. Technol.*, 2003, **172**, 217.

Figure caption:

Fig. 1 CV and LSV curves of Zn-Ni alloys on Pt electrode obtained from a') and a'') basic bath, b') and b'') basic bath with 15 mg/L CA, c') and c'') basic bath with 15 mg/L VL, d') and d'') basic bath with 15 mg/L CA and 15 mg/L VL.

Fig. 2 XRD patterns of Zn-Ni alloys electrodeposited from different baths: a) basic bath, b) basic bath with 15 mg/L CA, c) basic bath with 15 mg/L VL, d) basic bath with 15 mg/L CA and 15 mg/L VL.

Fig. 3 SEM images of Zn-Ni alloys deposited from different baths: a) basic bath, b) basic bath with 15 mg/L CA, c) basic bath with 15 mg/L VL, d) basic bath with 15 mg/L CA and 15 mg/L VL.

Fig. 4 AFM topographic images of Zn-Ni alloy coatings obtained from different baths, a) without additives, b) with additives (15 mg/L CA and 15 mg/L VL).

Fig. 5 Macroscopic images of Zn-Ni alloy coatings obtained from different baths, a) and c) without additives, b) and d) with additives (15 mg/L CA and 15 mg/L VL).

Fig. 6 Effects of different concentrations of: a) CA and b) VL on LSV curves.

Fig. 7 Effects of the concentration of: a) CA on Ni content and current efficiency of deposits obtained from the basic bath with 15 mg/L VL, and b) VL on Ni content and current efficiency obtained from the basic bath with 15 mg/L CA.

Fig. 8 XRD patterns of Zn-Ni alloys deposited from basic baths containing: a) different concentrations of CA with 15 mg/L VL, and b) different concentrations of VL with 15 mg/L CA.

Fig. 9 Effect of the composite additives (15 mg/L CA and 15 mg/L VL) on the hardness distribution of Zn-Ni alloy coatings.

Fig. 10 Variation of the friction coefficient of the Zn-Ni alloys with (15 mg/L CA and 15 mg/L VL) additives and without additives as a function of sliding distance.

599 **Fig. 11** XPS spectra of the original surface and a 10.0 nm depth of Zn-Ni alloy
600 deposits electrodeposited from the bath with composite additives: a) XPS general
601 spectra of the Zn-Ni alloys, b) high resolution peaks of N1s. c) high resolution peaks
602 of Zn2p, d) high resolution peaks of Ni2p, e) high resolution peaks of O1s from the
603 original Zn-Ni alloy surface, f) high resolution peaks of O1s after a 10.0 nm etching
604 of the original Zn-Ni alloy surface.

605 **Fig. 12** Polarization curves of Zn-Ni alloys obtained from the baths: a) with additives
606 (bright coating), b) without additives (dull coating).

Tables

Table 1

The electrochemical parameters (E_{corr}, i_{corr}, β_c, β_α) of deposits samples in a 3.5 wt.% NaCl solution.

Coatings	E_{corr} vs SCE /V	i_{corr}/μA·cm^{-2}	β_c/mV dec^{-1}	β_α/mV dec^{-1}
Bright coating	-0.801	37.15	228.62	63.53
Dull coating	-0.850	50.99	243.78	102.75
Steel	-0.475	21.10	204.08	40.39

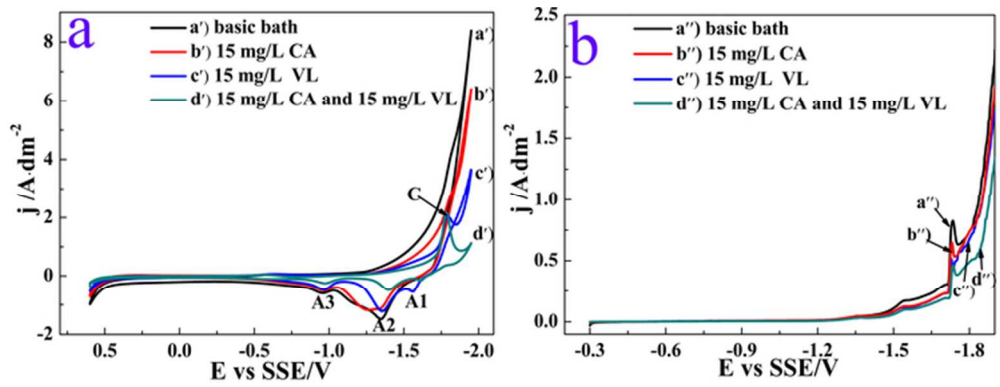

Fig. 1 CV and LSV curves of Zn-Ni alloys on Pt electrode obtained from a') and a'') basic bath, b') and b'') basic bath with 15 mg/L CA, c') and c'') basic bath with 15 mg/L VL, d') and d'') basic bath with 15 mg/L CA and 15 mg/L VL.
63x23mm (300 x 300 DPI)

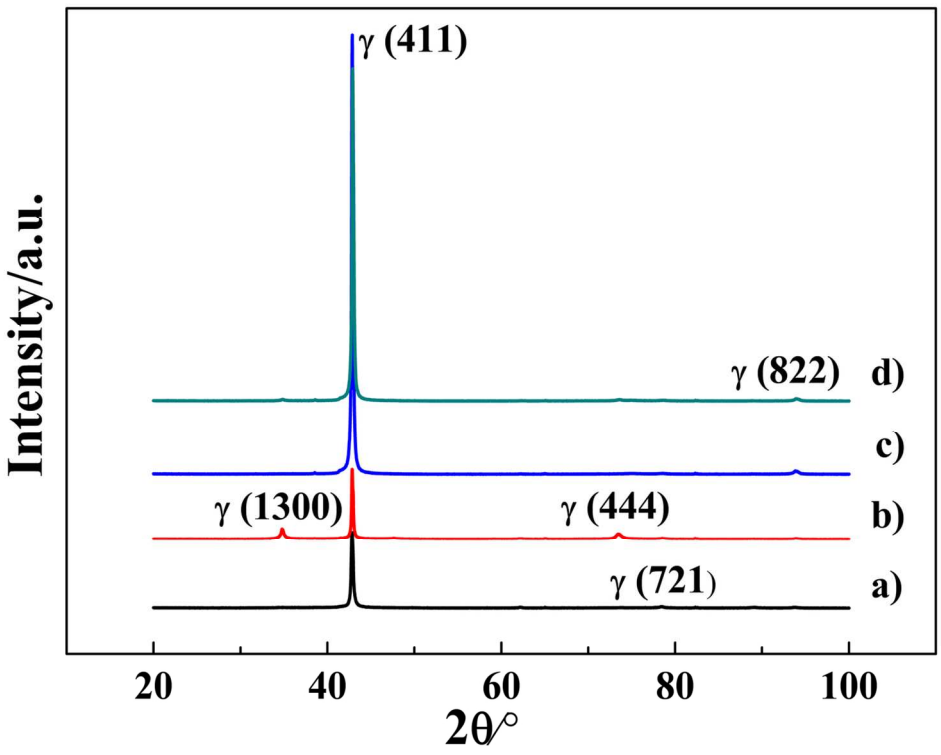

Fig. 2 XRD patterns of Zn-Ni alloys electrodeposited from different baths: a) basic bath, b) basic bath with 15 mg/L CA, c) basic bath with 15 mg/L VL, d) basic bath with 15 mg/L CA and 15 mg/L VL.
127x95mm (300 x 300 DPI)

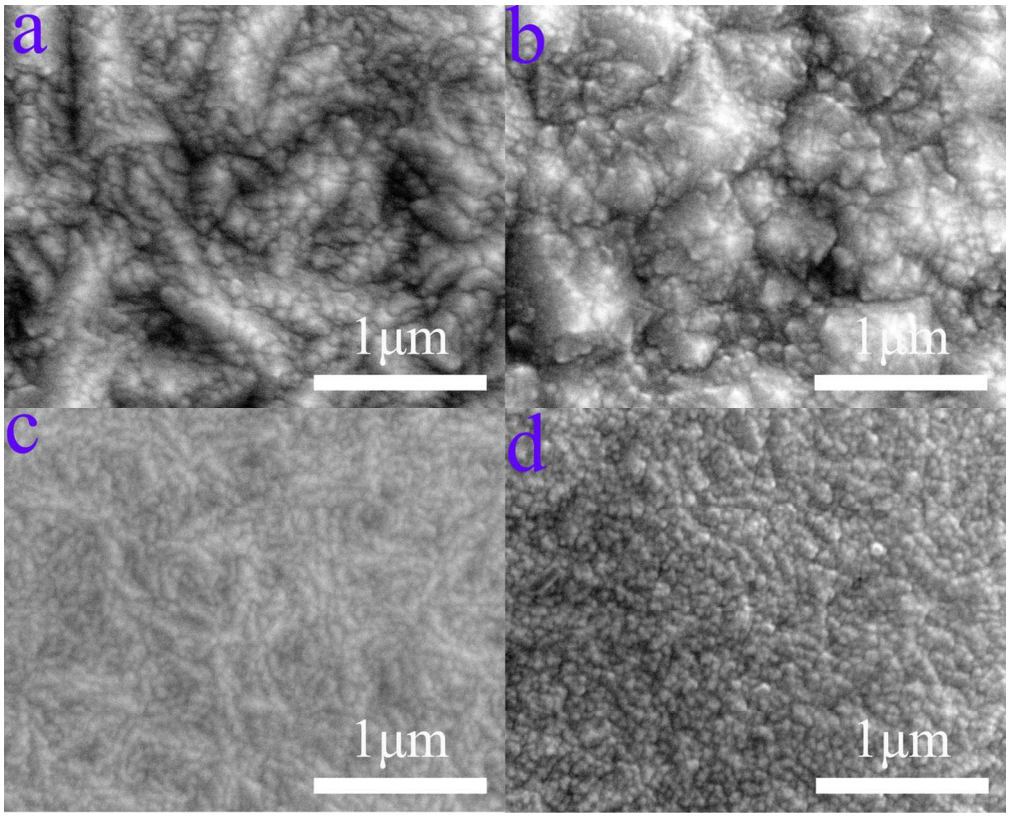

Fig. 3 SEM images of Zn-Ni alloys deposited from different baths: a) basic bath, b) basic bath with 15 mg/L CA, c) basic bath with 15 mg/L VL, d) basic bath with 15 mg/L CA and 15 mg/L VL.
124x100mm (300 x 300 DPI)

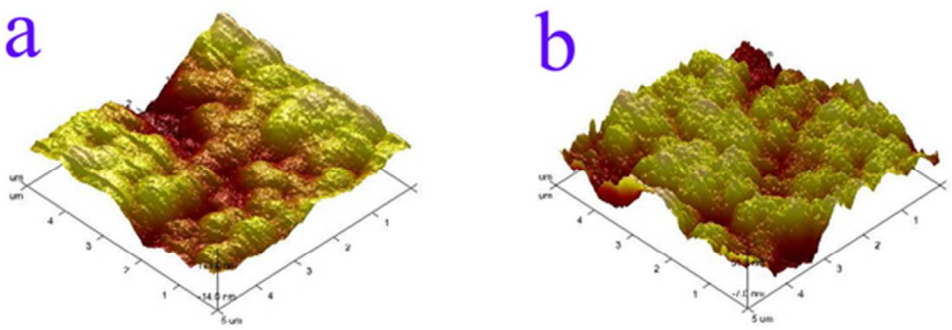

Fig. 4 AFM topographic images of Zn-Ni alloy coatings obtained from different baths, a) without additives, b) with additives (15 mg/L CA and 15 mg/L VL).
49x16mm (300 x 300 DPI)

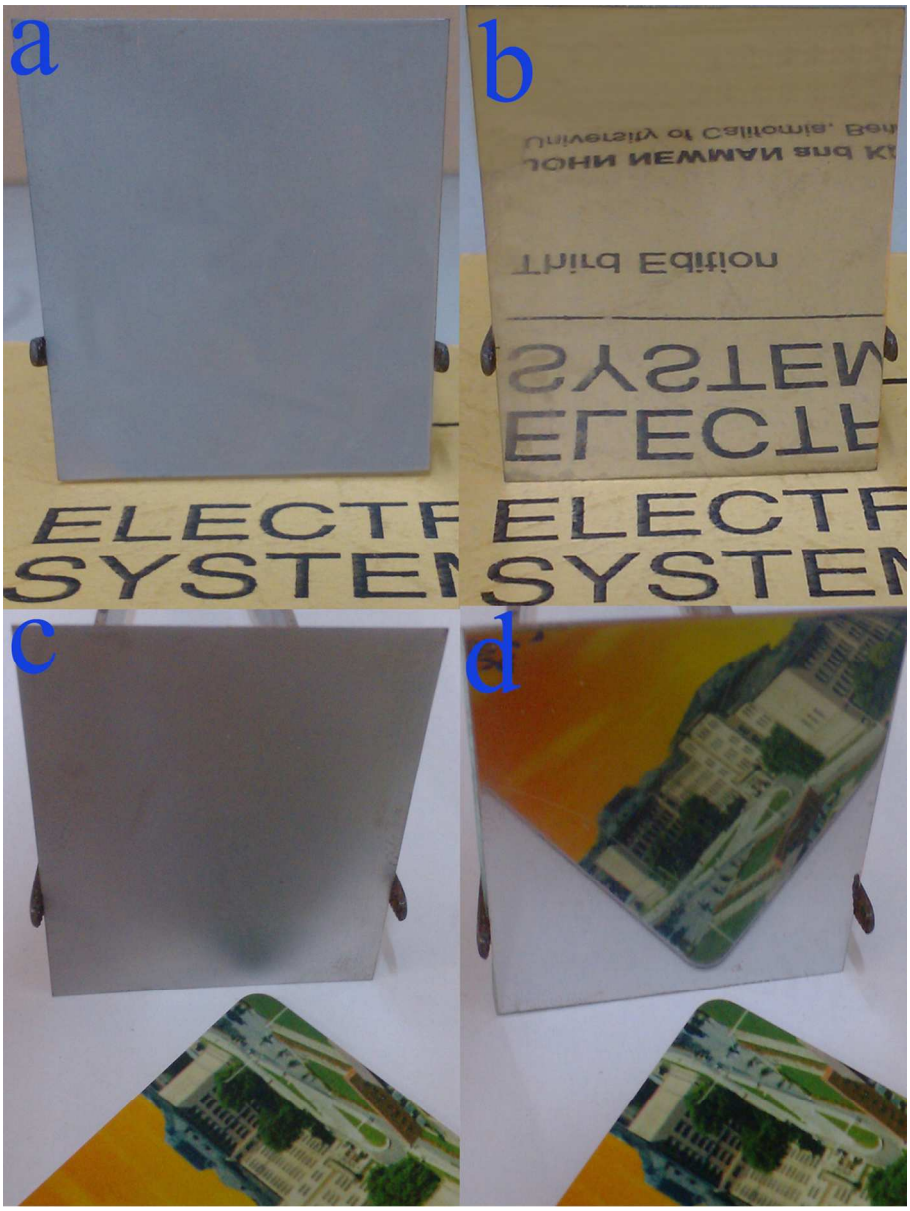

5 Macroscopic images of Zn-Ni alloy coatings obtained from different baths, a) and c) without additives, b) and d) with additives (15 mg/L CA and 15 mg/L VL).
127x168mm (300 x 300 DPI)

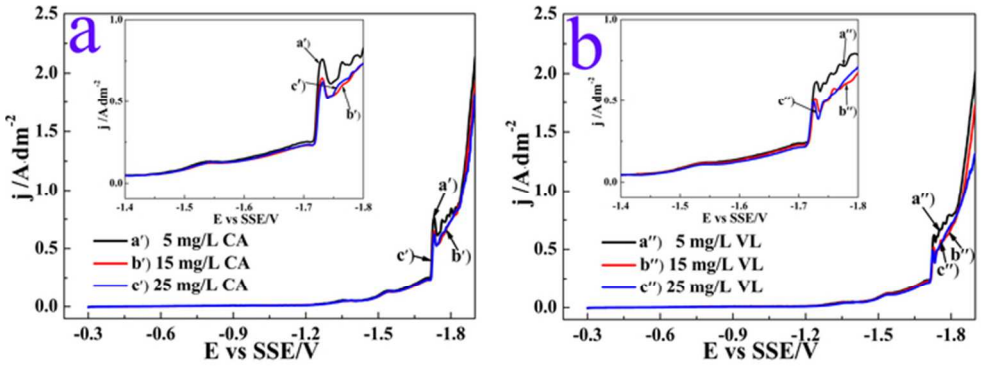

Fig. 6 Effects of different concentrations of: a) CA and b) VL on LSV curves.
63x23mm (300 x 300 DPI)

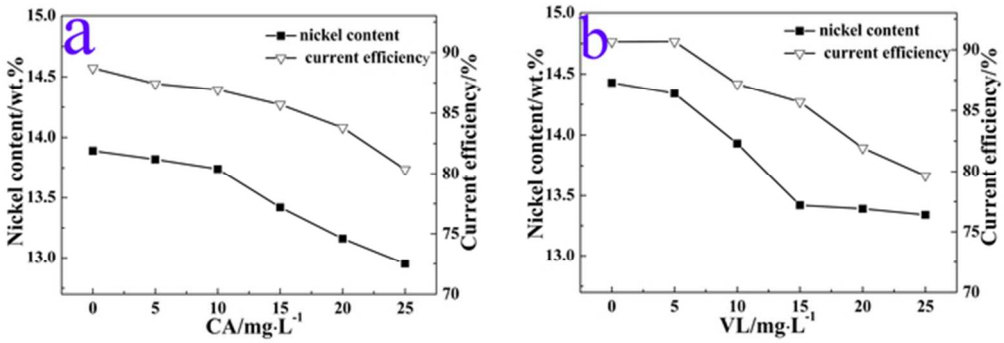

Fig. 7 Effects of the concentration of: a) CA on Ni content and current efficiency of deposits obtained from the basic bath with 15 mg/L VL, and b) VL on Ni content and current efficiency obtained from the basic bath with 15 mg/L CA.
57x19mm (300 x 300 DPI)

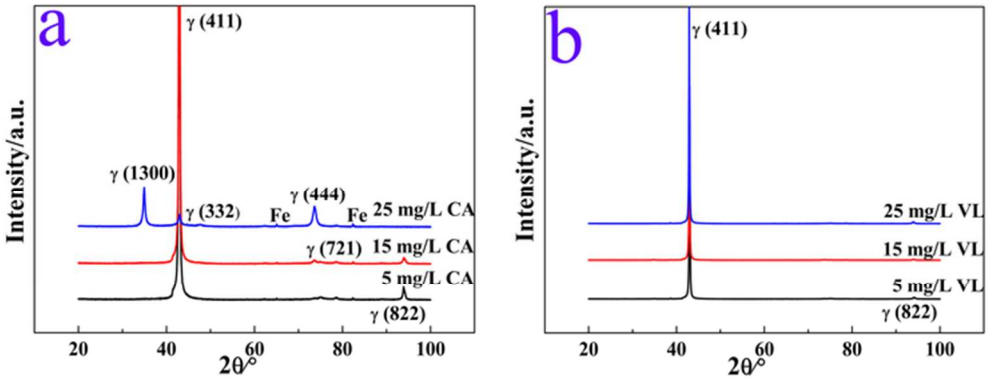

Fig. 8 XRD patterns of Zn-Ni alloys deposited from basic baths containing: a) different concentrations of CA with 15 mg/L VL, and b) different concentrations of VL with 15 mg/L CA.
63x23mm (300 x 300 DPI)

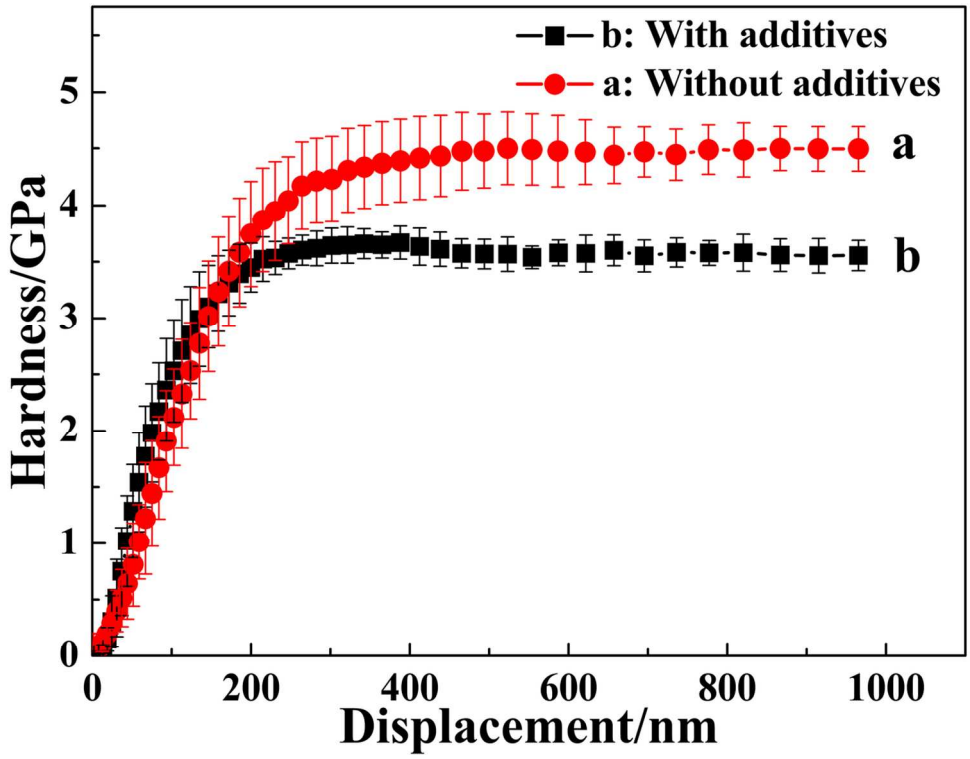

Fig. 9 Effect of the composite additives (15 mg/L CA and 15 mg/L VL) on the hardness distribution of Zn-Ni alloy coatings.
127x95mm (300 x 300 DPI)

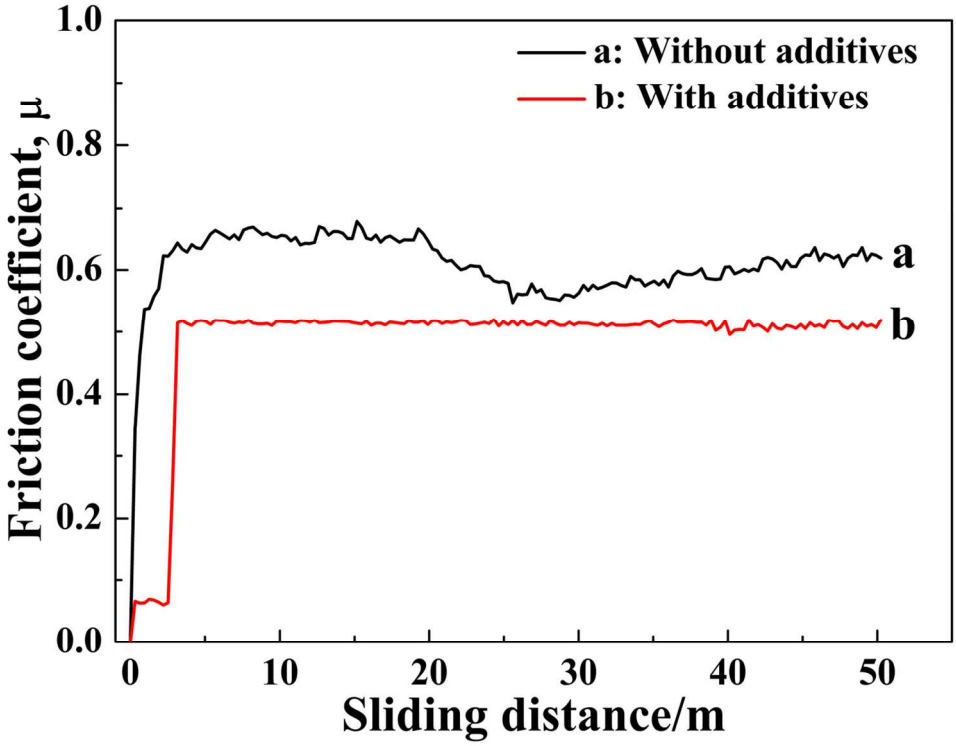

Fig. 10 Variation of the friction coefficient of the Zn-Ni alloys with (15 mg/L CA and 15 mg/L VL) additives and without additives as a function of sliding distance.
127x95mm (300 x 300 DPI)

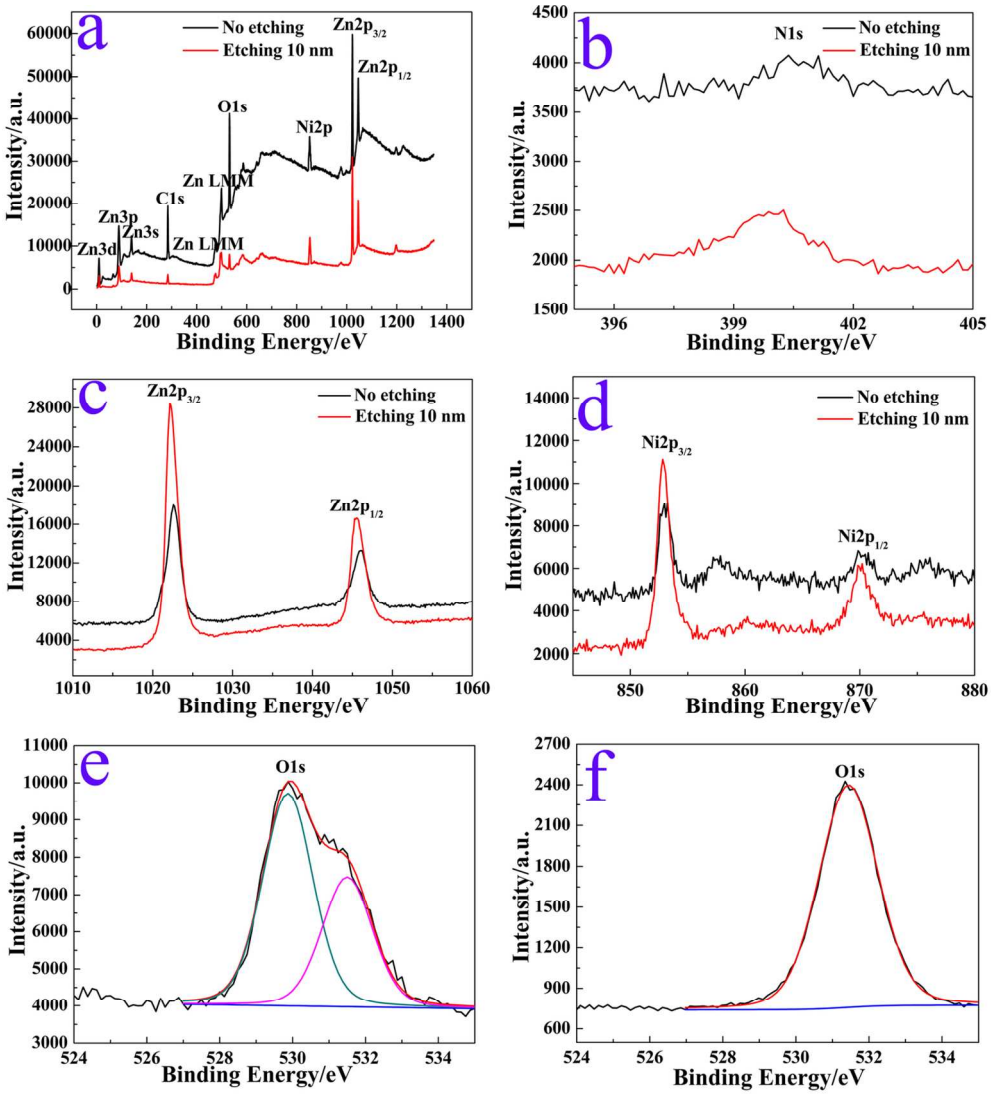

Fig. 11 XPS spectra of the original surface and a 10.0 nm depth of Zn-Ni alloy deposits electrodeposited from the bath with composite additives: a) XPS general spectra of the Zn-Ni alloys, b) high resolution peaks of N1s. c) high resolution peaks of Zn2p, d) high resolution peaks of Ni2p, e) high resolution peaks of O1s from the original Zn-Ni alloy surface, f) high resolution peaks of O1s after a 10.0 nm etching of the original Zn-Ni alloy surface.
127x139mm (300 x 300 DPI)

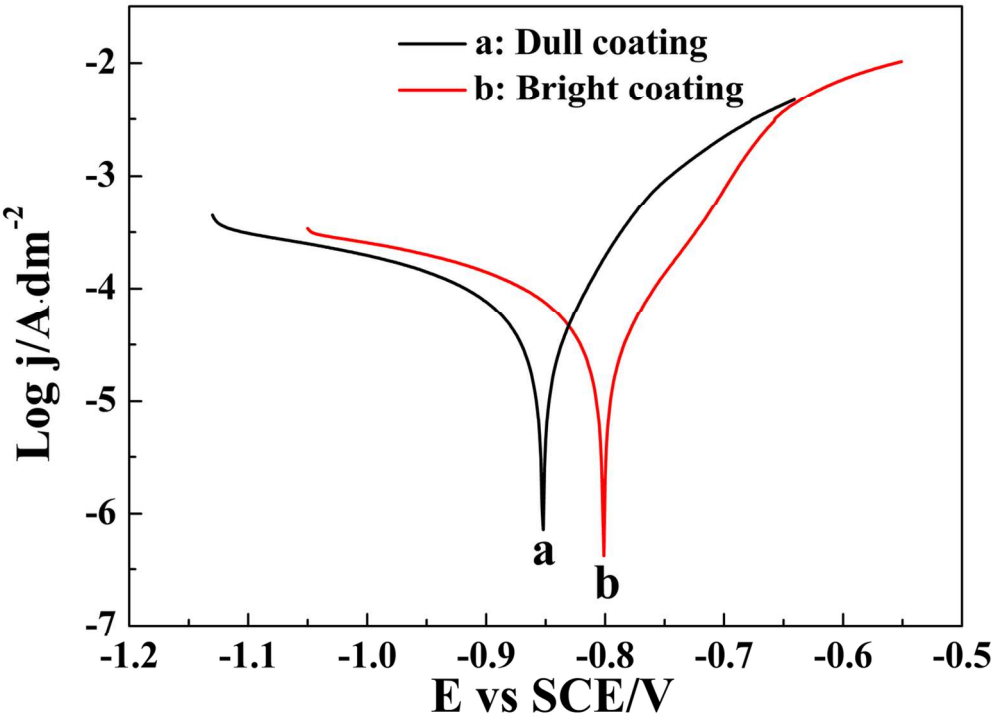

Fig. 12 Polarization curves of Zn-Ni alloys obtained from the baths: a) with additives (bright coating), b) without additives (dull coating).
127x95mm (300 x 300 DPI)